Secondary solitary wave formation in systems with generalized Hertz interactions

Felicia S. Manciu and Surajit Sen
Department of Physics, The State University of New York, University at Buffalo, Buffalo, New York 14260-1500
(Received 12 April 2001; revised manuscript received 12 April 2002; published 30 July 2002)

We consider a chain of monodisperse elastic grains of radius R where the grains are barely in contact. The grains repel upon contact via the Hertz-type potential, $V \propto \delta^n$, $n>2$, where $\delta \geqslant 0$, is the grain-grain overlap, $\delta \equiv 2R-(u_{i+1}-u_i)$, where u_i denotes the displacement of grain i from its original equilibrium position. This being a computational study, we consider n to be arbitrary. Our dynamical simulations build on several earlier studies by Nesterenko, Coste, and Sen and co-workers that have shown that an impulse propagates as a solitary wave of fixed spatial extent, $\infty < L(n) < 1$, through a chain of grains. Here, we develop on a recent study by Manciu, Sen, and Hurd [Phys. Rev. E **63**, 016614 (2001)] that shows that colliding solitary waves in the chains of interest spawn a well-defined hierarchy of multiple secondary solitary waves (SSWs) that carry $\sim$0.5% or less of the energy of the original solitary waves. We show that the emergence of SSWs is a complex process where nonlinear forces and the discreteness of the grains lead to the partitioning of the available energy into hierarchies of SSWs. The process of formation of SSWs involves length scales and time scales that are controlled by the strength of the nonlinearity in the system. To the best of our knowledge, there is no formal theory that describes the dynamics associated with the formation of SSWs. Calculations for cases where the Hertz-type potential can be symmetric in the overlap parameter δ, i.e., where δ can be both positive and negative, suggest that the formation of secondary solitary waves may be a fundamental property of certain discrete, nonlinear systems.

DOI: 10.1103/PhysRevE.66.016616 PACS number(s): 46.40.Cd, 45.70.−n, 43.25.+y

I. INTRODUCTION

The study of impulse propagation in a monodisperse chain of coupled elastic grains, which repel upon contact via the Hertz potential [1], can exhibit interesting nonlinear dynamics [2–5]. In the absence of external loading between the grains, the grains are barely in contact. It turns out that any impulse propagates as a solitary wave through such a chain of elastic grains [2–6]. The presence of loading destroys the solitary wave [2,3,7] and the solitary wave becomes dispersive as a function of the magnitude of loading [3]. The nature of dispersion is sensitive to the competition between the amplitude of the impulse and loading. Therefore, the zero-loading case is one of the most interesting regimes in which one can probe the nonlinear dynamical problem of impulse propagation in chains of elastic beads in contact. In this work, we consider monodisperse chains in the absence of external loading between the grains.

It should be mentioned here that for spherical grains in contact and for grains with conical imperfections, the Hertz potential is able to describe the interactions [1,8]. The Hertz potential describes power-law repulsion when grains are compressed and have no interaction otherwise. One can generalize the Hertz potential to study cases, which may not be easily realized in the laboratory and such an exercise can serve as a valuable tool to probe the general class of systems that interact via short-range power-law repulsive potentials. Examples of not easily realizable cases include Hertz potential with arbitrary power-law exponents and cases where the repulsive potential is introduced not only when the grains squeeze against each other but also when they are separated, i.e., a symmetric version of the Hertz potential. We call these cases Hertz-type potentials. These cases were not studied by Hertz in the context of elastic grains but are nevertheless of interest from the standpoint of nonlinear dynamics. Regardless of the details of the Hertz-type potential, it turns out that in the absence of loading, any impulse, no matter how weak, generates solitary waves in the chain of elastic grains [1–6].

It is well known that continuous wave acoustic signals, which can be obtained by sending an impulse in a chain of elastic grains under external loading, backscatter off buried inclusions in the chain of Hertzian grains [9]. In the absence of such loading, solitary waves also backscatter off impurities or inclusions in Hertzian chains [3]. Backscattering of solitary waves from buried inclusions in three-dimensional (3D) granular beds exhibit unusual behavior [10]. In the present study, we focus on an important idealization of the problem of backscattering of solitary waves, namely, one in which two identical solitary waves traveling in opposite directions meet one another at the geometric center of a chain with an odd number of grains. This problem is also identical to that of backscattering of a solitary wave from an infinitely massive impurity at the center of a chain and hence may reveal insights into the study of the general problem of backscattering of solitary waves from impurities [4].

This article is arranged as follows. Section II first presents the details of the model system (Sec. II A) and next summarizes the details of the integration algorithms used to carry out the calculations (Sec. II B). The studies on the crossing of solitary waves in a chain of discrete grains are presented in Sec. III. In Sec. III A we discuss our simulations that demonstrate the spawning of secondary solitary waves (see Manciu and co-workers [4]). This section is followed by Secs. III B and III C, where we present detailed discussions on the formation of secondary solitary waves [4] for the one-sided Hertz-type potential [1] and for symmetric versions of Hertz-type potentials [see Eqs. (1) and (2) below], respectively. Very little is presently known about the detailed dynamics

leading to the formation of secondary solitary waves. Computational limitations remain an important issue when studying the long time and spatial correlation effects that are typically associated with the formation of these objects. In Sec. IV, we summarize the present study.

II. MODEL SYSTEM AND ANALYSES

A. The model system

We consider a linear system of macroscopic, monodisperse beads of mass m and radius R. We let E and σ denote the Young's modulus and the Poisson's ratio, respectively. We assume that two such beads repel upon intimate contact according to Hertz's law [1]. We define the overlap $\delta_{i,i+1} \equiv \Delta-(u_{i+1}-u_i)$, where u_i denotes the displacement of grain i from the equilibrium position and $\Delta=2R-\eta$, η being the loading of the chain (grain compression prior to the generation of the impulse). For spherical beads, the repulsive Hertz potential [1] is given by

$$V(\delta_{i,i+1}) = (\tfrac{2}{5}D)(R/2)^{0.5}\delta_{i,i+1}^{n} \equiv a\,\delta_{i,i+1}^{n} \quad \text{if} \quad \delta_{i,i+1}\geqslant 0$$
$$\equiv 0 \quad \text{if} \quad \delta_{i,i+1}<0, \tag{1}$$

where $D\equiv\frac{3}{2}(\{1-\sigma^2\}/E)$ and $n=\frac{5}{2}$. If $n\to 2$, the repulsive force approaches the harmonic limit ($n=2$). In general, the constant a depends upon the material parameters (E and σ) and the magnitude of n depends upon the contact geometry between the beads. It turns out that typically n varies between $n=\frac{5}{2}$ and 3 [8]. We assume that the signal propagates through each grain at a speed that is significantly slower than the velocity at which sound wave propagates through each bead. We also ignore the energy lost to internal degrees of freedom in each grain, i.e., we ignore restitutive losses. Restitutional loss leads to exponential attenuation of the amplitude of the propagating pulse and can be incorporated into the analyses. However, our studies show that restitutional losses (modeled as outlined above) do not affect the width of the solitary wave but simply attenuates the amplitude of a propagating solitary wave in an exponential manner. It is therefore convenient to ignore such losses and treat our system as a conservative system for our present objective, namely, for studying the dynamics of secondary solitary waves. Due to the nonlinear nature of the repulsion between adjacent grains, one might expect that dynamical phenomena involving compression and decompression of grains would be highly nonlinear in nature. Since the Hertz potential is asymmetric, additional effects occur because the grains can lose contact for periods of time. In order to probe the effects of nonlinearity alone, we also studied the problem with the interaction described by a symmetric Hertz potential,

$$V(\delta_{i,i+1}) = a|\delta_{i,i+1}|^{n}. \tag{2}$$

The equation of motion of some bead i (excluding the edge grains) in a finite chain of Hertzian beads is given by

$$m d^2u_i/dt^2 = na\{[\Delta-(u_i-u_{i-1})]^{n-1} - [\Delta-(u_{i+1}-u_i)]^{n-1}\}. \tag{3}$$

Initially, every grain is placed barely in touch with one another such that $\Delta=2R$. We call this the no-loading case. An impulse defined by an initial velocity v_0 at time $t=0$ is initiated at the first bead [2,3]. As the impulse propagates, one finds via numerical, experimental, and analytical studies that a solitary wave develops in space and time [2–6].

We outline the procedure for constructing an approximate solution for $u_i(t)$ in Eq. (3). With reference to earlier studies [3–7] and the results from numerical simulations, we start by assuming that our system admits a solitary wave solution. We further assume that the displacement of individual grains from equilibrium position $u_i(t)$ are continuous functions of time but are defined only at discrete positions z_i. Since the solitary wave is nondispersive, we can assume that this displacement can be obtained from a wave-type continuous function of both space and time, from the relation

$$u_i(t)=u(z_i,t)=u(z_i-ct)=u(\alpha) \quad \text{with} \quad \alpha=z-ct, \tag{4}$$

where c is the constant velocity of the solitary wave.

Our exhaustive numerical studies on Eq. (3) and also other work indicate that, for a given n, the shape of the solitary wave in space does not depend on the solitary wave amplitude. This implies that the function u is described by $u(\alpha)=A\psi_n(\alpha)$, where A represents the amplitude of the solitary wave and where one can set $A=u(-\infty)-u(+\infty)=1$. The quantity $\psi_n(\alpha)$ is an unknown generic function that describes the shape of the solitary wave and is expected to depend upon the index n, which controls the stiffness of the potential. Because the solitary wave is localized in space, $\psi_n(\alpha)$ should be necessarily zero for $\alpha\to\infty$ ($z\to\infty$ for finite t, which represents a region that the solitary wave is yet to reach) and 1 for $\alpha\to-\infty$ (where grains have attained a new equilibrium position after the passage of the compression produced by the tsunami-like or kink solitary wave). A function that respects this boundary condition and can only take intermediate values between 0 and 1, can be always written as

$$\psi_n(\alpha)=1/(1+\exp)[f_n(\alpha)], \quad \text{with}$$
$$f_n(\alpha)=\ln[1/\psi_n(\alpha)-1]. \tag{5}$$

With this notation, the solitary wave function becomes

$$u(\alpha)=A/2[\varphi_n(\alpha)+1] \quad \text{with} \quad \varphi_n(\alpha)=\tanh[f_n(\alpha)/2]. \tag{6}$$

One can see from Eqs. (4)–(6) that $du/dz|_t = -(1/c)du/dt|_z$. Substituting Eq. (6) into Eq. (3), we get, for $t=0$,

$$mc^2/na(A/2)^{n-2} = [\{\varphi_n(z-2R)-\varphi_n(z)\}^{n-1} - \{\varphi_n(z) - \varphi_n(z+2R)\}^{n-1}]/[d^2\varphi_n/dz^2] \equiv C_0(n), \tag{7}$$

where the left-hand side is independent of z and the right-hand side is independent of m, a, and A. Thus, C_0 should be

independent of z, m, a, and A, which means that C_0 is a constant that depends only on n.

Equation (7) implies that $\varphi_n(z)$ is antisymmetric with respect to $z=0$, which is the center of solitary wave (recall that t was set to zero). This fact, combined with the asymptotic limits for $\psi_n(z)$ and Eq. (5) indicates that

$$f_n(z)=\sum_{q=0}^{\infty} C_{2q+1}(n)z^{2q+1}. \tag{8}$$

Since the function $\varphi_n(z)$ does not depend upon the solitary wave amplitude or material parameters (except for interaction power n), knowledge of the coefficients C_0, C_1, C_3, C_5,..., will completely solve the problem of pulse propagation for any system supporting this type of solitary wave. In the absence of a simple analytical approach for inferring C_0 and C_{2q+1}, one must resort to numerical methods for computing these coefficients.

Recall that Eq. (7) implies that

$$c=\{naC_0(n)/m\}^{1/2}(A/2)^{(n-2)/2}, \tag{9}$$

which implies that the propagation velocity of the solitary wave scales with its amplitude except when $n\rightarrow 2$, the harmonic limit, where c becomes independent of amplitude, as expected. As we shall see, the velocity of the solitary waves become very weakly dependent on n as $n\rightarrow 2$.

The width of the solitary wave, $L(n)$, turns out to be sensitive to n and to the grain diameters. When one considers monodisperse chains, n is the only parameter that controls the width of the solitary waves. When $n\rightarrow\infty$, $L(n)\rightarrow 1$. When $n\rightarrow 2$, $L(n)\rightarrow\infty$, i.e., the system no longer accommodates a solitary wave [2,4]. The behavior of $L(n)$ vs n is illustrated in Fig. 1(c). For the most common case with n between 2.5 and 3, the solitary waves are about three grain diameters wide.

B. The integration algorithm

The calculations reported in this study have been carried out using the sixth-order Gear predictor-corrector algorithm [11]. In our numerical calculations we used $m=1$, $a=1$, $v_0=1$ (imparted initial velocity). Observe that in a system with no external loading, the repulsive forces are purely nonlinear and Eq. (3) cannot be linearized. In all of our studies reported in Secs. III B and III C, the chains have 999 grains and the integration time step used is $dt=1.3\times 10^{-2}$ for the asymmetric potential and $dt=9.75\times 10^{-3}$ for the symmetric potential. The time step used was identical for studies for all values of n. In all of our calculations, the number of time steps was 100 000. The total energies during the runs were typically constant to an accuracy of about 0.02%.

Two identical solitary waves are created by imparting the same initial velocity (v_0 and $-v_0$) to the first and last grains of the chain. The symmetry with the central grain is always preserved, which implies that the central grain is always at rest for all the simulations. The problem is identical to that of backscattering of a solitary wave by a grain with infinite mass.

III. THE CROSSING OF IDENTICAL SOLITARY WAVES

A. Secondary solitary waves

We first summarize the study in which *two solitary waves* of the same amplitude but opposite displacements are initiated at the two ends of a chain with 499 grains. The system is set up in such a way that the solitary waves meet one another at the *center* of the central grain of the chain, i.e., at grain number 250. It should be mentioned that the results of collision between solitary waves may be slightly different if they do not collide at the center grain but at an arbitrary point along the line joining a grain center to the contact point between two grains. Systematic studies on ''off-center'' (i.e., symmetry broken) collisions, which are more challenging to probe than the current study in which only grain centers are involved, will be carried out at a later stage.

An important question to address is whether at the point of intersection, the opposing solitary waves ''cancel out,'' i.e., whether the center of the central grain suffers any motion at any time. In earlier numerical analyses of limited precision carried out by Nesterenko [2], it was found that the solitary waves underwent perfect annihilation at the point of crossing. As we shall see, improved resolution of the calculated data reveals that there is no motion of the central grain at any time and that there is significant motion of the elastic grains in the immediate vicinity of the central grain. Figure 1(a) shows a drawing of the process of collision between two opposite propagating solitary waves in a chain of elastic grains.

In Fig. 1(b), we present the kinetic energy versus distance (measured in grain diameter) and time. One can see that the grains that are adjacent to grain number 250 begin to oscillate or ''rattle,'' breaking mutual contact and reestablishing contact again in the process. Such rattling eventually gives rise to the generation of multiple solitary waves of progressively diminishing amplitudes, which move at progressively slower velocities. We call these waves, ''secondary'' solitary waves (SSWs).

The process of formation of SSWs involves a complex sequence of grain-grain compressions between two, three, and perhaps more adjacent grains in certain time sequences. These processes remain to be analytically resolved. However, it is possible to develop some intuition about the formation of SSWs via the following arguments that are based upon a simplified description of the dynamics of grains in the immediate vicinity of the collision point. Assume that a solitary wave hits an infinitely massive central grain, say grain number $N+1$ in a $2N+1$ grain chain. We recall from the discussion in Sec. II A that a typical solitary wave in a chain of spherical grains with $n=2.5$ is about three grain diameters wide with the bulk of its energy at the geometric center of the solitary wave. As the solitary wave impinges upon the central grain, the Nth grain would simply reflect off the $(N+1)$th grain. However, the grain that is two grains apart from the center of the $(N+1)$th grain would not suffer such a reflection after a time $2R/c$ (where c is the speed of the entire solitary wave). Grain $N-1$ would continue to squeeze grain N when grain N might be moving in opposition to grain $N-1$ with an acceleration that is controlled by the reflection

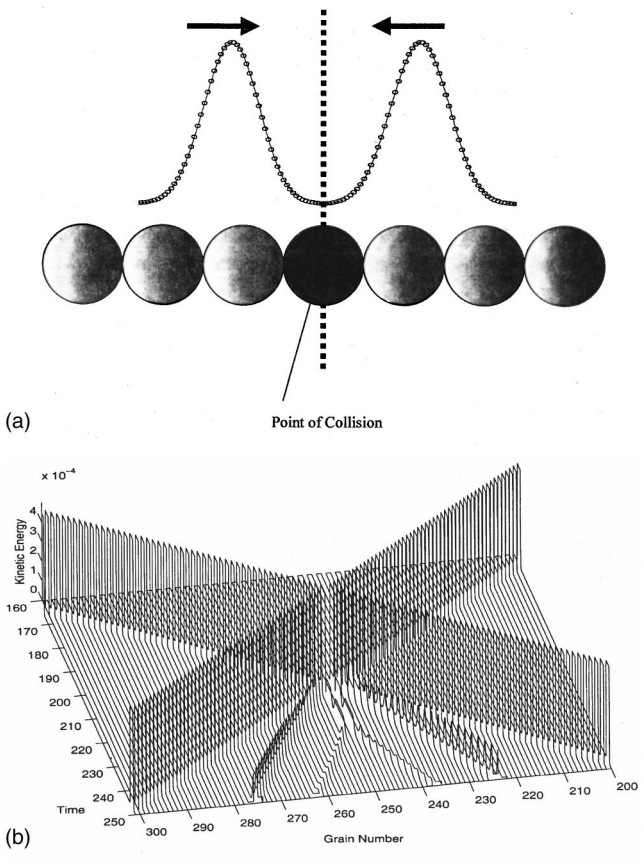

FIG. 1. (a) The drawing shows the central part of a chain of elastic beads. The center grain is dark. The velocities of the two opposite propagating solitary waves are shown. The data points are obtained from dynamical simulations and the continuous fits are obtained using the solution to the equation of motion in Sen and Manciu in Ref. [4]. (b) The plot shows kinetic energy along the *z* axis and time and space (in terms of grain diameter or grain number) along *x* and *y* axes, respectively. Two solitary waves collide at the center of grain number 250 in a chain of 499 grains. The emergence of the first two secondary solitary waves can be seen.

against grain $N+1$. While one can pursue the grain dynamics in this fashion, it is clear that the time scales associated with the compression of grains during the propagation of a solitary wave of finite size is significantly altered by the presence of the static central grain. Given that in a chain of grains interacting via the Hertz potential, any perturbation must propagate as a solitary wave, the original solitary wave must be destroyed by the central grain and will have to be reconstructed. This process of reconstruction of the original solitary wave leads to the formation of the reflected solitary waves and SSWs.

B. Complex hierarchies of secondary solitary waves: Asymmetric Hertz-type potentials

We study the formation and propagation of secondary solitary waves in monodisperse Hertzian chains. The analyses are shown by recording the maximum compression between any two adjacent grains and the maximum velocity of the grains as functions of time. The data are shown in Figs. 2–6. In each case, the upper panel [labeled (a)] shows data on the maximum compression between any two adjacent grains as a function of time. The lower panel [labeled (b)] shows data on the velocities of the grains. It turns out that it is difficult to meaningfully represent the data when the magnitude of some dynamical variable (such as position or velocity) as a function of space and time is being shown without making three-dimensional plots. It turns out that three-dimensional plots tend to be too complicated to decipher the detailed dynamics of the system being probed. To keep our presentation simple, we record the minimum distance between the adjacent grains along the *y* axis and place circles of appropriate diameter to indicate the window within which the magnitude of the grain-grain distances lie (please refer to Table I).

In a Hertzian chain with zero loading, the propagation of the solitary wave can be tracked either by recording the maximum velocity of the particle or the maximum compression between the grains. In our simulations, we first consider the case where the Hertz-type potential is such that it produces a steep repulsion upon compression. To achieve such a steep repulsion, we set $n=3$, in other words, we make the potential more abruptly repulsive than the usual case of $n=\frac{5}{2}$ for spherical grains in contact. These data are shown in Fig. 2. It turns out that the width of the solitary wave is slightly larger than a single grain diameter for $n=3$ [4].

Before the collision, these points yield the line with the negative slope at the left of each of the panels in Figs. 2(a)–6(a). In each of these figures, this negatively sloped line represents the *incoming solitary wave* towards the center of the chain as a function of time. The data reveal that the slope of the incoming wave becomes smaller as *n* is lowered from 3.0 to 2.1. This result implies that the solitary wave moves progressively slower as *n* is lowered in magnitude [see Eq. (9)]. The part of the solitary wave that is ''reflected'' at the collision point by the infinitely massive center is clearly visible to the immediate right of the incoming solitary wave in Figs. 2(a)–6(a). The reflected wave possesses very nearly the same magnitude as the incoming wave. Nevertheless, the incoming and reflected waves are not perfectly symmetric with respect to the normal dropped onto the time axis at the point of collision, thereby indicating that the incoming and reflected solitary waves have slightly different velocities. The asymmetry can be readily seen in the Figs. 2(a)–6(a). The calculations suggest that the part of the kinetic energy that is not available to the reflected solitary wave ends up being used to make SSWs.

The data in Figs. 2–6 clearly show that after the collision between two identical solitary waves (or the reflection of a solitary wave from an infinite central mass), some energy *remains temporarily localized* in the immediate vicinity of the point of collision. The localization time increases as $n \to 2$, eventually becoming divergent in the limit $n=2$, where $L(n) \to \infty$. This localized energy leads to the rattling of the grains starting from the immediate vicinity of the collision point. The process of rattling lasts across extended time and length scales, controlled by *n*. The process of multiple collisions between the grains as the grains lose and regain contact in the immediate vicinity of the collision point leads to the

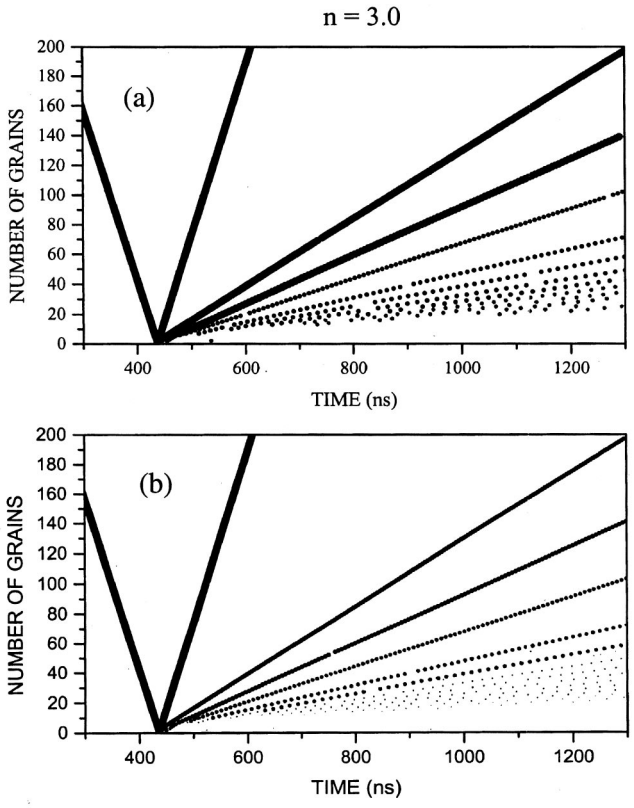

FIG. 2. We show half of a chain of 999 grains. Incoming solitary wave (negative slope line on the left of the panel) backscatters off the center of the chain and makes some 11 SSWs of decreasing amplitudes, moving at progressively slower speeds. In (a), the compression pulses are characterized by smallest distance between adjacent grains described by $u_{i+1}(t)-u_i(t)|_{(\text{minimum value})}$. When the magnitude of compression between two adjacent grains lie within a chosen range (see Table I), we record the compression with the appropriate symbol. In (b) the same system is shown by plotting the relative velocities of each grain with respect to the one in front versus time.

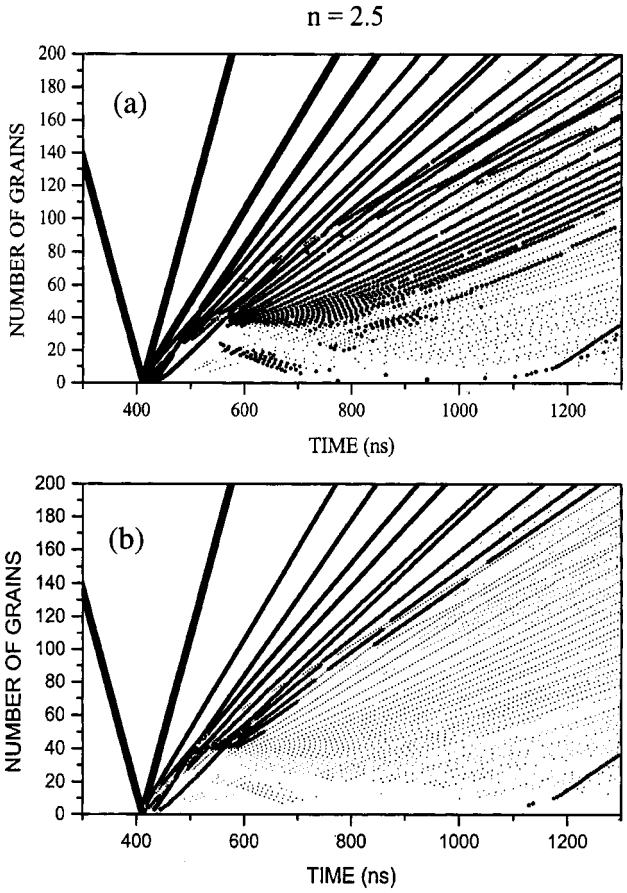

FIG. 3. The information represented is the same as in Figs. 2(a) and 2(b) except that we study the case with $n=2.5$. Physically, $n=2.5$ corresponds to a chain of spherical beads. Softening of the potential allows for the production of many more SSWs. Observe that both forward and backward propagating SSWs form in this system.

formation of the secondary solitary waves. Given that typical solitary waves for n between 3 and 2.5 or so are about three grain diameters wide, three-grain motion in unison is necessary for the system to construct SSWs. The evolution of such correlated motion depends upon n and hence the formation and propagation of SSWs as shown in Figs. 2(a), 2(b) to 6(a), 6(b) are so strongly n dependent. It turns out that in softer potentials, the contact period between the grains in a typical collision is more long lived than for $n=2.5$ and 3. Thus, systems with softer potentials yield more SSWs [2–6]. Of course, while the SSWs have the same width as the normal solitary waves in Hertz chains discussed in Sec. II, their amplitudes are much smaller and hence they propagate much slowly [see Eq. (9)] compared to the amplitudes of the original solitary waves that produce these secondary solitary waves. Since the velocities of the SSWs are dependent upon their amplitudes, they correspondingly move more slowly than the solitary waves. In most of our studies, we find that the energy trapped in the secondary solitary waves is about 0.5% of the original energy associated with the two colliding solitary waves [4].

If one looks at the velocity extrema plots in cases where the one-sided Hertz potential is considered, meaning the case in which the grains do not interact when they lose contact [Figs. 2(b)–6(b)], the data reveal that it takes secondary solitary waves several time units to form after the collision event. This is due to the fact that the grains lose contact after the collision and move with constant velocity between individual impacts. In order to have an extremum in velocity, *at least three grains should be in contact simultaneously*. On the other hand, minima in the distances between the adjacent grains represent impacts between individual grains, regardless of the position of the other grains of the chain. It is evident that it takes sufficient time and sufficient number of grain-grain collisions to make secondary solitary waves, as we have emphasized above.

In the vicinity of the collision point, the extrema appears to be somewhat random, which suggests that the motion of the adjacent grains after the crossing of the solitary waves is presumably highly complex in nature. However, after a certain period of time, the system accommodates the available energy into a hierarchy of secondary solitary waves. When a secondary solitary wave is completely formed, the maxima

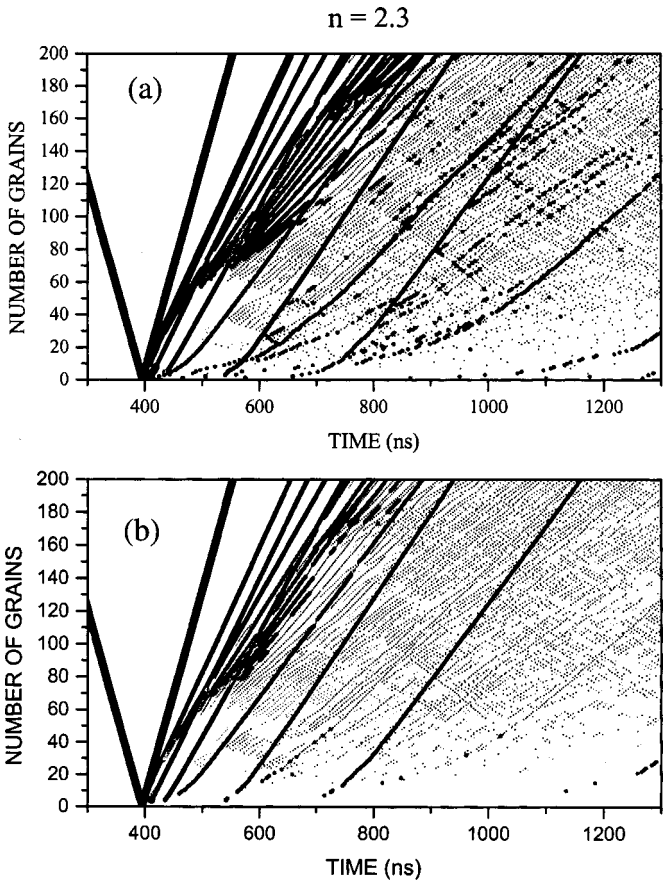

FIG. 4. The information represented is the same as in Figs. 2(a) and 2(b) except that we study the case with $n=2.3$. Physically, $n=2.3$ corresponds to a chain of spherical beads. Softening of the potential allows for the production of many more SSWs. Lowering the value of n leads to slower velocities [see Eq. (9)] of the SSWs.

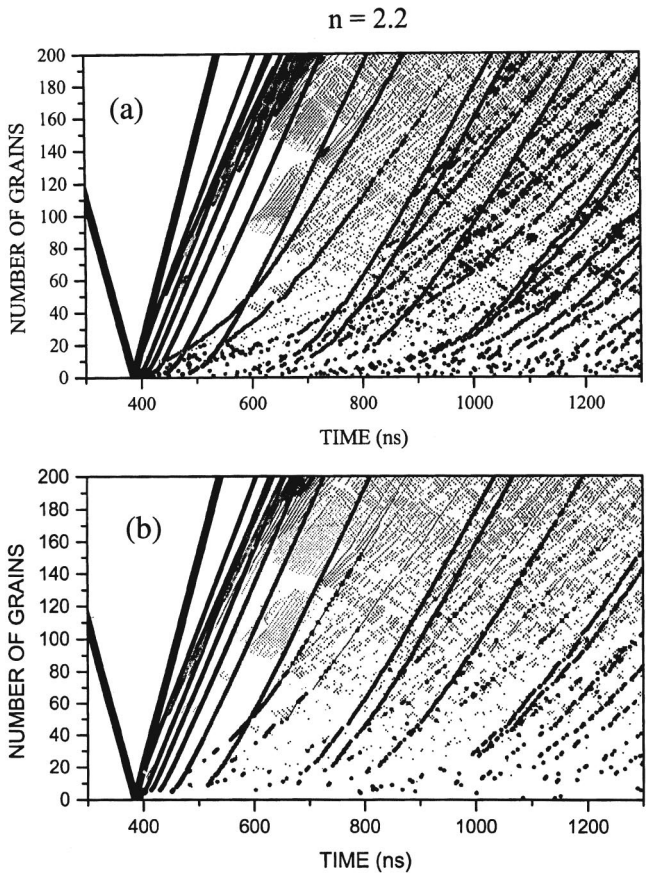

FIG. 5. The information represented is the same as in Figs. 2(a) and 2(b) except that we study the case with $n=2.2$. Softening of the potential allows for the formation of more dominant SSWs.

are again organized on a line, whose slope is related to the velocity of the secondary solitary wave and hence to the solitary wave energy [4].

In Fig. 3, we report calculations carried out for the case $n=2.5$. The lower value of n implies that the Hertz-type potential is less repulsive than for the $n=3$ case. Comparison with the data in Fig. 2 readily reveals that many more secondary solitary waves are formed across a long period of time, which is an expected result when the repulsive potential is softened, thereby making it easier for three grains to collide in such a way that SSWs can form more frequently. Figure 3(a) shows data in which the compressions between the adjacent grains are presented as a function of time. Figure 3(b) shows the grain velocities as a function of time for the study shown in Fig. 3(a). The data in the upper and lower panels reveal interesting branching features, which indicate that SSWs can be generated from SSWs themselves (see, for example, data points at $t\sim500$, grain number ~20, $t\sim700$, grain number ~80, etc.). It should be noted that SSWs, once formed, move at fixed velocities that depend upon their amplitudes according to Eq. (9). Thus, when one plots the minimum distance between the adjacent grains as a function of time, one is tracking the propagation of a compression pulse and hence the emergence and the propagation of a SSW. The plot of the minimum distances between adjacent grains versus time as shown in Figs. 2(a)–6(a) shows linear trajectories beyond some time after their formation. The tendency of the trajectories to make progressively smaller angle with respect to the time axis reveals that the majority of the solitary waves that form at late times move more slowly than those that form at earlier times. There are cases when fairly strong SSWs form at late times [see Figs. 4(a) and 5(a)] and intersect the slower moving weaker waves that may have formed earlier. Our calculations appear to suggest that we find SSWs as they are forming.

Continuing in the same way, one expects that the process of generation of secondary solitary waves would become progressively more complex as n decreases. Figures 4(a), 5(a), and 6(a) present grain-grain compression and grain velocity data for $n=2.3$, 2.2, and 2.1, respectively. It is computationally difficult to carry out calculations in the vicinity of the harmoniclike $(n\rightarrow2)$ limit. The softness of the potential leads to extended time scales across which the adjacent grains are in contact, and in turn leads to extended time and length scales across which large numbers of SSWs can form. Figure 6(a) suggests that weak SSWs that propagate in the direction of the original incoming solitary wave may also be formed. Furthermore, after formation, these waves move exceedingly slowly and take a relatively long time to make SSWs. In the absence of a lower limit on the energy carried

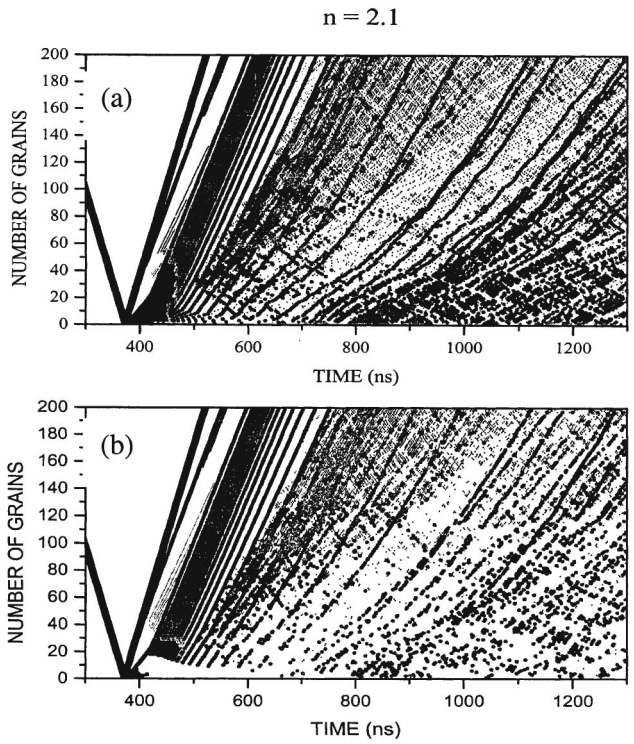

FIG. 6. The information represented is the same as in Figs. 2(a) and 2(b) except that we study the case with $n=2.1$, the closest case to the harmonic limit ($n=2$) that we could study in detail. With decreasing n it is evident that the SSWs tend to propagate at very nearly the same velocity. In the limit $n\rightarrow 2$, all excitations are expected to move at the same speed.

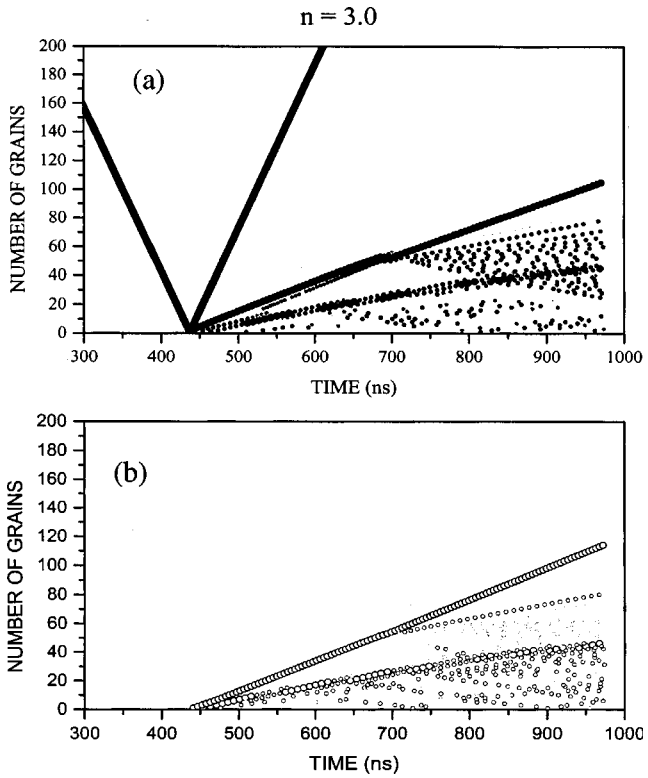

FIG. 7. As in Fig. 2(a), in both the panels we show the process of collision of two opposite propagating solitary waves by depicting half of a 999 grain chain where the grains interact via the symmetric Hertz potential [Eq. (2)] for $n=3.0$. Figure 7(a) shows the dynamics of SSWs while Fig. 7(b) shows the dynamics of SASWs. The SSWs and SASWs show almost identical propagation patterns stemming from the fact that SSWs and SASWs form in pairs.

by a SSW, it is likely that secondary solitary waves continue to spawn indefinitely from the point of crossing of two solitary waves.

There is no simple scaling behavior that we are able to identify that can be used to describe the hierarchy of magnitudes of these secondary solitary waves versus the sequence of the solitary wave. If one considers Fig. 4(a) or 4(b) and draws a horizontal line, starting, say, at grain number 200, it is evident that there are large amplitude solitary waves that form at late times. The data in Figs. 5 and 6 present convincing evidence of formation of large amplitude secondary solitary waves at late times, i.e., after the formation of many weak SSWs. For any given value of n there are varied time scales across which SSWs can form. Formation of SSWs is not a simple, scale invariant, sequential process.

C. Complex hierarchies of secondary solitary waves: Symmetric Hertz-type potentials

In this section, we study the process of crossing of two identical, opposite-propagating solitary waves in the ''symmetric Hertz-type potential'' as described via Eq. (2). This potential allows for a nonvanishing force even when two adjacent grains are not in contact with one another (much like in a harmonic potential except that the potential is nonlinear). As stated earlier, we keep the loading parameter $\eta=0$. The change in the potential allows for the propagation of *both solitary waves and antisolitary waves* in the system, where by a solitary wave one implies a compression pulse and by an antisolitary wave one means dilation pulse.

One expects different behavior during the collision between two opposite propagating solitary waves in this system. Of course, as we have seen above, interactions between solitary waves in these discrete systems spawn SSWs. In the symmetric problem, in addition to the secondary solitary waves, the system also spawns secondary antisolitary waves (SASWs). Figures 7 ($n=3$), 8 ($n=2.5$), 9 ($n=2.3$), 10 ($n=2.2$), and 11 ($n=2.1$) describe the dynamical behavior of the distance between adjacent grains versus time when solitary waves [Figs. 7(a)–11(a)] and antisolitary waves are formed [Figs. 7(b)–11(b)]. Observe that there is no incoming antisolitary wave in Figs. 7(b)–11(b). The magnitudes of the displacements and velocities are qualitatively indicated in terms of solid (for solitary waves and SSWs) and open (for antisolitary waves and SASWs) circles and via their respective gray scales. Table I also explains the magnitudes associated with the gray scale that has been used. The dynamical evolution of maximum compression between adjacent grains as a function of time turns out to be a more accurate indicator of time evolution in the symmetric systems.

It is interesting to see that in all of the Figs. 7–11, the symmetry of the potential allows the formation of forward propagating SSWs (i.e., moving in the same direction as the original solitary wave that hit the infinite wall in the half

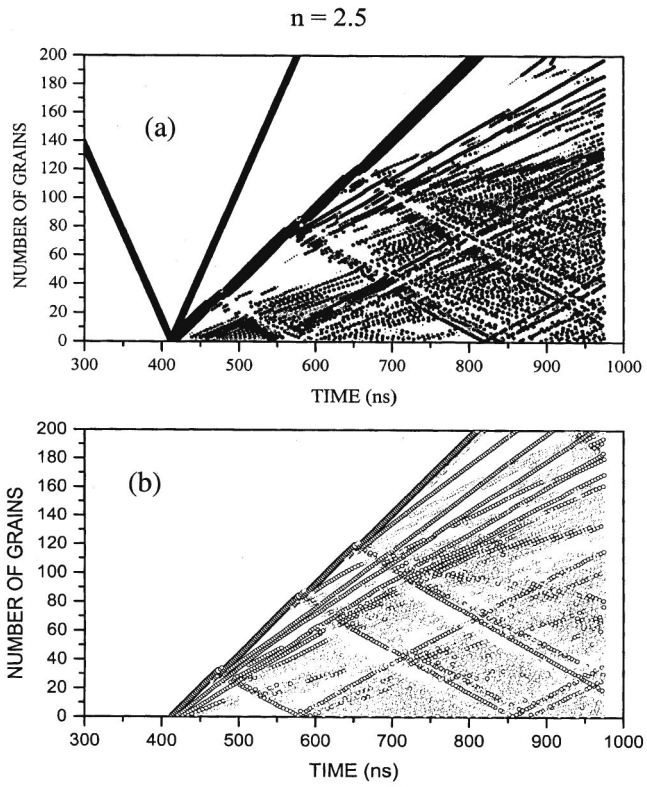

FIG. 8. The information presented is identical to that in Figs. 7(a) and 7(b) except that $n=2.5$. As in Fig. 3, softening of the potential introduces more SSWs and SASWs in the post collision era.

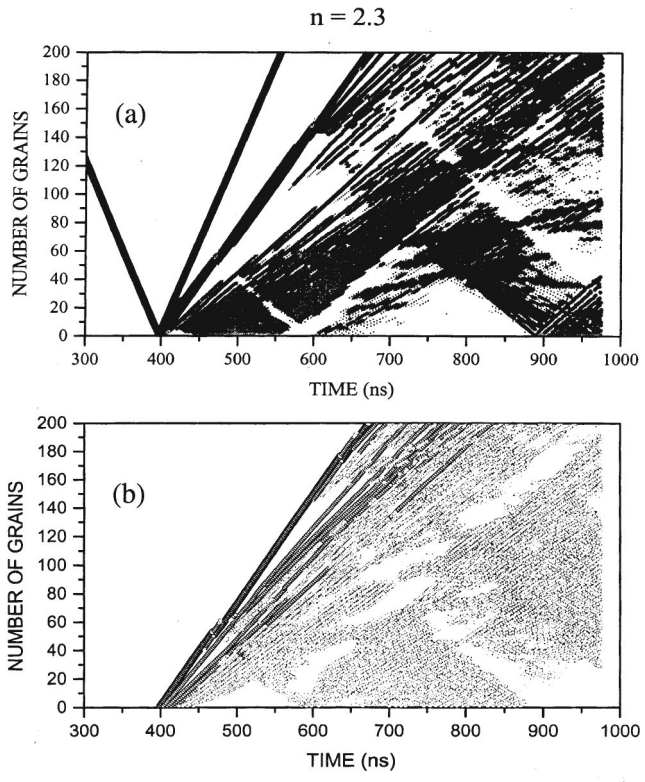

FIG. 9. The information presented is identical to that in Figs. 7(a) and 7(b) except that $n=2.3$. The data reveals that at later times there are phases (e.g., between $t\sim600$ and 900 ns, grain numbers 1–40 and beyond) in which the system makes only SASWs.

chain) and backward propagating SSWs (i.e., moving in the direction opposite to that of the original solitary wave that hit the infinite wall in the half chain). To see the backward propagating secondary solitary waves, the reader may note the negatively sloped lines in Figs. 7(a)–10(a). These detailed features are smoothened and largely outside the range of data shown for the case $n=2.1$ in Fig. 11, in which the spatial width of the solitary wave is rather large. The rapid increase in $L(n)$ between $n=2.2$ and $n=2.1$ bears testimony to the significant differences in the two figures. Identical features are also visible for *antisolitary* waves. The number of SSWs and SASWs generated grows rapidly to form continuumlike structures in the graphs as $n\rightarrow2$ [see, for instance, Figs. 10(a), 10(b), 11(a), and 11(b)]. The process of formation of secondary solitary and antisolitary waves become progressively more short ranged and hence in rapid intervals as n decreases. Examination of long-range and late-time data on SSWs and SASWs reveal that the dynamical behavior of individual grains far from the collision point is, for all practical purposes, chaotic.

IV. DESCRIPTION OF A TYPICAL TRAJECTORY OF COMPRESSION PULSE

In Fig. 12 we have reexamined the data describing the process of formation of the first seven SSWs for a specific case, namely, $n=2.2$ case shown in Fig. 5(a). We have extracted the points that record the maximum compression between the adjacent grains as a function of time and space for each SSW that we study. According to the discussions presented in Sec. II A, the maximum compression is a fixed number for a given SSW. The data shows that initially the maximum compression between the grains behaves as a nonlinear function. In time, the compression pulse starts to propagate at constant speed and becomes a propagating solitary wave. We have fitted the data for each SSW with a time-dependent function that possesses a linear piece in time and a hyperbolic function in time. The linear piece in time is introduced to model the observed behavior that the compression pulses must propagate at uniform speeds, if they are to be identified with solitary waves. The formation of a compression pulse, as seen in constructing solution to the equation of motion of the grains [4,6], is best described by a $\tanh f(t)$ function. A functional form that is consistent with the properties associated with the displacement of the grains as alluded to in Eq. (6) and that fits the data is

$$u_{i+1}(t)-u_1(t)\big|_{\text{minimum value}} = I+P_1(t-t_0)-P_2\tanh[P_3(t-t_0)], \quad (10)$$

where P_1, P_2, and P_3 are constants that vary with the order of the solitary wave. The constant t_0 represents the time of collision between the two solitary waves.

Table II presents the values of parameters as a function of the order of the solitary wave. The first five secondary solitary waves are well formed in the data displayed. Table II

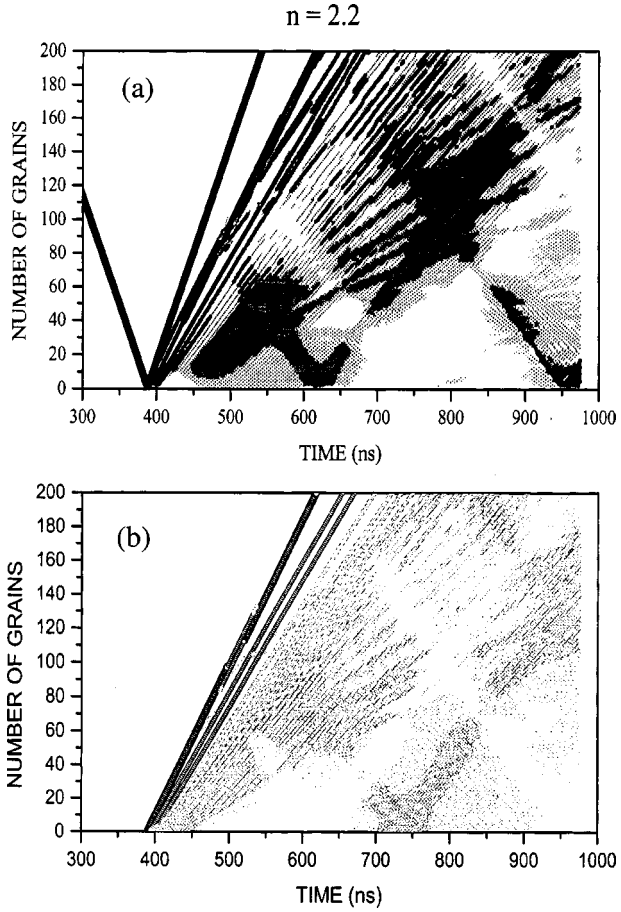

FIG. 10. The information presented is identical to that in Figs. 7(a) and 7(b) except that $n=2.2$. The resolution of our data suggests band formation of the SSWs and SASWs.

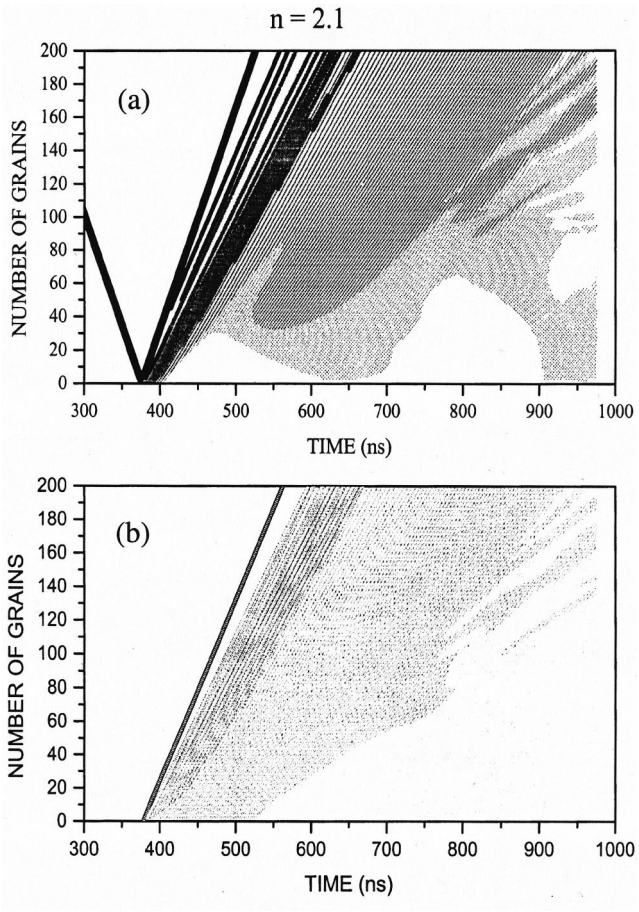

FIG. 11. The information presented is identical to that in Figs. 7(a) and 7(b) except that $n=2.1$. In the region near the collision point, the formation of SSWs and SASWs reveal different features whereas their propagation behavior is similar at larger distances from the collision point.

reveals that the coefficient P_1 decreases linearly for the first five SSWs with the order of the SSW, thus reconfirming that the secondary solitary waves of higher order propagate more slowly. The sixth and seventh SSWs are still in the process of formation at $t\sim900$ and grain diameter 100 and hence the coefficients P_1, P_2, and P_3 for these cases cannot be compared with those for the first five SSWs. The coefficient P_2 controls the early time dynamics of the compression pulse. In cases where the compression pulse rapidly assumes propagation at uniform speed, P_2 is the weakest. SSWs 6 and 7 do not end up propagating at uniform speeds in Fig. 12, which is evident if one observes the fitted curves having one's line of vision aligned with the data points. The coefficient P_3 controls rate of growth of the curves at early times and is anoma-

TABLE I. Magnitude of relative displacements and velocities of grains in arbitrary units for solitary waves (dark circles) and antisolitary waves (open circles) shown in Figs. 2–11.

		●	>	1×10^{-1}
1×10^{-3}	<	●	<	1×10^{-1}
5×10^{-4}	<	●	<	1×10^{-3}
1×10^{-4}	<	●	<	5×10^{-4}
1×10^{-7}	<	·	<	1×10^{-4}
		○	>	1×10^{-1}
1×10^{-3}	<	○	<	1×10^{-1}
5×10^{-4}	<	○	<	1×10^{-3}
1×10^{-4}	<	●	<	5×10^{-4}
1×10^{-7}	<	·	<	1×10^{-4}

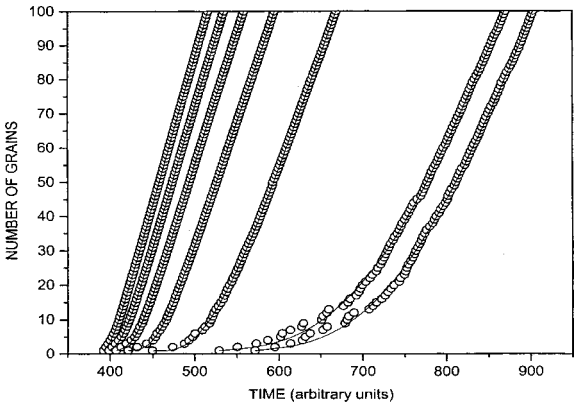

FIG. 12. Data showing the spatiotemporal evolution of the first seven secondary solitary waves in the $n=2.2$ case. The fitted curves are discussed in the text.

TABLE II. Least squares fits using Eq. (10) for data presented in Fig. 12.

	χ^2	P_1	P_2	P_3
Sec. Sol. 1	0.006 56	0.857 41 ± 0.000 32	7.304 29 ± 0.026 23	0.079 14 ± 0.000 93
Sec. Sol. 2	0.011 68	0.813 ± 0.000 45	12.027 22 ± 0.041 99	0.054 4 ± 0.000 52
Sec. Sol. 3	0.015 9	0.773 03 ± 0.000 55	18.022 1 ± 0.059 84	0.039 35 ± 0.000 3
Sec. Sol. 4	0.030 96	0.733 61 ± 0.000 88	28.573 09 ± 0.119 85	0.025 64 ± 0.000 19
Sec. Sol. 5	0.081 09	0.692 54 ± 0.002 09	53.303 24 ± 0.417 91	0.013 28 ± 0.000 11
Sec. Sol. 6	0.791 08	0.807 1 ± 0.028 3	201.151 28 ± 13.414 51	0.003 93 ± 0.000 14
Sec. Sol. 7	0.856 45	0.780 13 ± 0.026 33	180.471 64 ± 11.822 19	0.004 21 ± 0.000 15

lously dominant for the two weakest secondary solitary waves. These are the reasons why the coefficients P_1, P_2, and P_3 for these two cases do not follow the trend established by the first five secondary solitary waves.

V. SUMMARY AND CONCLUSION

In this paper we have presented a study of the dynamical processes associated with the collision of two opposite propagating solitary waves in 1D systems with the grains interacting via asymmetric Hertz-type [1] potentials and via symmetric Hertz-type potentials. The studies have been carried out under conditions of zero external loading of the chains. In systems with Hertz-type potentials, it is possible to generate compressive pulses, i.e., pulses in which the distance between the grains attain a minimum, which in turn propagates through the chain at a constant speed. Such a compression pulse turns out to be a solitary wave. The speed depends upon the amplitude of the pulse via Eq. (9). In systems with asymmetric Hertz-type potentials, it is possible to generate both compression and dilation pulses. The dilation pulse turns out to be an antisolitary wave.

Our calculations have been carried out by numerically integrating the equation of motion for each grain for each of these potentials. The computations involved were performed with extremely high precision and were carried out over 5 decades in time steps to ensure that the smallest and the slowest moving energy bundles could be detected in our studies. Figures 2(a)–6(a) show the data obtained by recording the maximum compression between the adjacent grains (some fixed number) as functions of space and time, before and after the collision of two identical, opposite propagating solitary waves. The grain velocities are plotted as functions of time in Figs. 2(b)–6(b).

Our data indicate that after the collision between two identical solitary waves, a small part of the total energy in the two original solitary waves remains in the collision point. This energy then starts to spread outward in both directions. These nonlinear physical systems automatically partition this energy into a hierarchy of SSWs, which form over extended time and length scales in an overall decreasing order in magnitude. Thus, larger SSWs form relatively rapidly after the collision and across smaller length scales (except when n is close enough to 2). For $n \gg 2$, the length scales across which the largest SSWs form are relatively small, being typically several grain diameters. When $n \to 2$, the length scale across which the largest SSWs form exceeds more than 40 grain diameters. The number of weak SSWs grows dramatically as n is lowered. Time scales and length scales associated with the formation of these weak SSWs become comparable to the time and length scale across which the simulations have been performed. This trend suggests the possible onset of a divergence in time and length scales associated with the formation of secondary solitary waves as $n \to 2$.

ACKNOWLEDGMENT

The research has been supported by NSF Grant No. CMS-0070055.

[1] H. Hertz, J. Reine Angew. Math. **92**, 156 (1881).

[2] V. F. Nesterenko, J. Appl. Mech. Tech. Phys. **5**, 733 (1983); V. F. Nesterenko, J. Phys. IV **C8**, 729 (1994); G. Friesecke and J. A. D. Wattis, Commun. Math. Phys. **161**, 391 (1994); V. F. Nesterenko, A. N. Lazaridi, and E. B. Sibiryakov, J. Appl. Mech. Tech. Phys. **36**, 166 (1995); R. S. Sinkovits and S. Sen, Phys. Rev. Lett. **74**, 2686 (1995); S. Sen and R. S. Sinkovits, Phys. Rev. E **54**, 6857 (1996); C. Coste, E. Falcon, and S. Fauve, *ibid.* **56**, 6104 (1997); E. J. Hinch and S. Saint-Jean, Proc. R. Soc. London, Ser. A **455**, 3201 (1999); R. S. MacKay, Phys. Lett. A **251**, 191 (1999).

[3] S. Sen, M. Manciu, and J. D. Wright, Phys. Rev. E **57**, 2386 (1998); A. Chatterjee, *ibid.* **59**, 5912 (1999); E. Hascoët, H. J. Herrmann, and V. Loreto, *ibid.* **59**, 3202 (1999); S. Sen, M. Manciu, R. S. Sinkovits, and A. J. Hurd, Granular Matter **3**, 33 (2001).

[4] S. Sen and M. Manciu, Physica A **268**, 644 (1999); M. Manciu, S. Sen, and A. J. Hurd, Phys. Rev. E **63**, 016614 (2001).

[5] M. Manciu, S. Sen, and A. J. Hurd, Physica A **274**, 588 (1999); **274**, 607 (1999).

[6] S. Sen, M. Manciu, F. S. Manciu, and A. J. Hurd, in *Powders and Grains 01*, edited by Y. Kishino (A. A. Balkema, Rotterdam, 2001); S. Sen and M. Manciu, Phys. Rev. E **64**, 056606 (2001).

[7] J. Hong, J. Y. Ji, and H. Kim, Phys. Rev. Lett. **82**, 3058 (1999); M. Manciu, V. Tehan, and S. Sen, Chaos **10**, 658 (2000); J.

Hong and A. Xu, Phys. Rev. E **63**, 061310 (2001).
[8] D. A. Spence, Proc. R. Soc. London, Ser. A **305**, 55 (1968); K. L. Johnson, *Contact Mechanics* (Cambridge, New York, 1985).
[9] For recent studies, see C. J. Hickey, J. M. Sabatier, and T. M. McGee, Ann. Geofis. **43**, 1225 (2000).
[10] M. Manciu, S. Sen, and A. J. Hurd, in *The Granular State*, edited by S. Sen and M. L. Hunt, Mater. Res. Soc. Symp. Proc. 627, No. BB3.4 (Materials Research Society, Pittsburgh, 2001); S. Sen, M. Manciu, K. Campbell, J. Schein, R. Prasad, and M. Krishnan, Proc. SPIE **4394**, 607 (SPIE, Bellingham, WA, 2001).
[11] M. P. Allen and D. J. Tildesley, *Computer Simulation of Liquids* (Oxford, New York, 1987).